ACS Combinatorial Science

RESEARCH ARTICLE

pubs.acs.org/acscombsci

Sequentially Modified, Polymer-Stabilized Gold Nanoparticle Libraries: Convergent Synthesis and Aggregation Behavior

Matthew I. Gibson,† Maarten Danial, and Harm-Anton Klok*

Ecole Polytechnique Fédérale de Lausanne (EPFL), Institut des Matériaux and Institut des Sciences et Ingénierie Chimiques, Laboratoire des Polymères Bâtiment MXD, Station 12, CH-1015 Lausanne, Switzerland

Supporting Information

ABSTRACT: This manuscript describes a versatile, yet experimentally facile, method for producing libraries of polymer-coated (core−shell type) gold nanoparticles. The synthetic principle relies on two, sequential postmodification reactions, which ensures homogeneity across each series. First, poly(pentafluorophenyl methacrylate) synthesized by RAFT polymerization is used here as a reactive precursor, which can be modified, postpolymerization, to create a library of functional polymers each bearing a ω-thiol end-group. In a second step, these well-defined polymers are then tethered by their ω-thiol group to the surface of prefabricated citrate-stabilized gold nanoparticles to give a library of 75 unique, yet sequentially modified organic−inorganic hybrid particles. The optical properties of the gold core were exploited to create a high-throughput assay for investigating the role of nanoparticle size and surface coating on aggregation in various biologically relevant media. These experiments demonstrated the importance of the type of dissolved salts present and also the strong influence of serum proteins in cell-culture media and their interactions with nanoparticles surfaces, which in turn might affect their biological profiles. Therefore, this method presents a powerful, yet accessible tool for creating model nanoparticle libraries with intrinsic sensing properties.

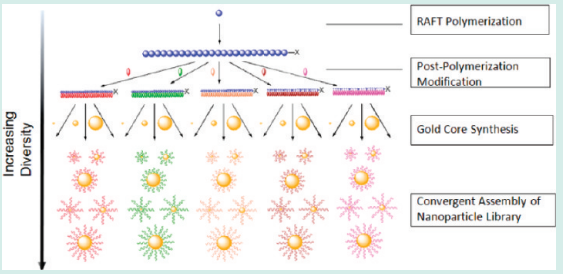

KEYWORDS: polymer-stabilized, gold nanoparticle libraries, RAFT polymerization, biologically relevant media

INTRODUCTION

Nanoparticles have attracted significant interest in biology and medicine as imaging or diagnostic tools or for drug delivery applications, to name a few.[1−3] In spite of the widespread interest, a fundamental understanding of the basic physicochemical characteristics that determine nanoparticle toxicity, as well as cell uptake, trafficking, and body distribution, is still lacking at the moment.[4] As a consequence, at the current state-of-the-art, it is a challenge to de novo design nanoparticles with predictable properties. The need for nanoparticle structure−activity relationships is further driven by societal concerns over the potential environmental and toxicological impact of nanomaterials.[4,5] To establish structure−property relationships, high-throughput synthetic strategies are needed that allow facile access to diverse nanoparticle libraries with precise control over nanoparticle size and surface chemistry.

Nanoparticles can be produced using a variety of strategies including block copolymer self-assembly,[6] precipitation,[7] or cross-linking[8] strategies, as well as via surface modification of metal-(oxide) nanoparticles.[9] A very attractive materials platform for the production of nanoparticle libraries, especially from a biological/medical point of view, are gold nanoparticles. Gold nanoparticles are of interest for a number of reasons. First of all, gold nanoparticles are easily prepared using well-established methods, which allow precise control over their size and shape.[10,11] Second, their physicochemical properties can be adjusted by immobilization of low molecular weight thiols or thiol end-functionalized polymers.[12−14] Since it does not require covalent bond formation and is extremely functional group tolerant (apart from Michael-type acceptors and thiols, most other functional groups will not interfere), this surface modification method allows a mix-and-match synthesis of nanoparticle libraries and would be compatible with automated or high-throughput methods. Third, and in addition to the synthetic advantages, gold nanoparticles can be analyzed using inductively coupled plasma atomic emission spectroscopy[15,16] and imaged with TEM or X-ray tomography,[17] which are attractive to (quantitatively) study nanoparticle uptake and distribution. Last, but not least, gold nanoparticles have unique optical properties, which depend on particle size and shape as well as interparticle interactions. The aggregation-sensitive optical properties of gold nanoparticles have been used, for example, to detect specific DNA sequences,[18] to monitor lectin binding by carbohydrates,[19] to probe enzymatic activity,[20] to detect metal ions[21] or pH changes,[22] or to monitor temperature-responsive particle aggregation.[23]

There are several reports of the in situ reduction of gold salts in the presence of polymers containing thiol, disulfide, or thioether end-groups to create polymer-coated gold nanoparticle libraries. These methods typically lead to relatively small (<4 nm)

Received: December 28, 2010
Revised: January 30, 2011
Published: March 08, 2011

nanoparticles with the actual diameter varying according to the polymer used.[24−26] Alternatively, gold nanoparticles can be modified with polymers by the "grafting from" approach using controlled radical polymerization.[23,27] In several recent reports the pharmaceutical properties of small, poly(ethylene glycol) (PEG) coated gold nanoparticle libraries are discussed.[28] Perrault et al. demonstrated that tuning nanoparticle size and PEG length can influence the selective in vivo tumor targeting potential of the nanoparticles. Whereas 100 nm particles were found to accumulate near the blood vessels, 20 nm particles could distribute throughout the tumor. Increasing the PEG molecular weight from 2000 to 10000 $g \cdot mol^{-1}$ also resulted in significantly increased blood half-lives, demonstrating that both the intrinsic size and the coating of nanoparticles contribute to their biological behavior.[29] These studies are not only valuable as they provide fundamental insight into the basic physicochemical characteristics that underlie the biological properties of these particles, but also as they serve as model experiments that can provide guidelines for the design of polymer nanoparticles with predictable biological properties.

In this contribution, we report a new, facile, convergent strategy for the synthesis of diverse, polymer-coated gold nanoparticle libraries. The proposed strategy is based upon the use of a reactive polymer precursor, which is prepared by reversible addition−fragmentation chain transfer (RAFT) polymerization and which can be postmodified to generate libraries of side-chain functional polymers with identical chain lengths and chain length distributions.[30] The thiol end-groups of these polymers can subsequently be used for their immobilization onto gold nanoparticle surfaces. The strategy proposed here has several distinct advantages compared to the PEG-coated gold nanoparticle platforms reported so far. First of all, the post-polymerization modification of a side-chain reactive polymer precursor greatly enhances the chemical diversity that can be accessed in comparison to the PEG-coated particles where chemical modification is essentially limited to the PEG chain end. A second advantage of the use of well-defined side-chain reactive polymer precursors and post-polymerization modification is that it allows a systematic variation of surface chemical functionalities (e.g., charge, polarity), while keeping all other parameters, such as gold nanoparticle size and size distribution, as well as chain length and chain length distribution of the tethered polymers constant. This report describes the results of a first proof-of-concept study in which 25 different polymers with varying chain length and functionality were immobilized onto 3 different citrate stabilized gold nanoparticles to generate a 75-member particle library. The optical properties of the gold nanoparticle cores were subsequently used to develop high-throughput assays in which the aggregation stability of the polymer coated nanoparticles in several biologically relevant media was studied.

EXPERIMENTAL PROCEDURES

Materials. Gold(III) chloride trihydrate ($HAuCl_4$; > 49% Au, ACS grade), sodium chloride (>99%), and thiol terminated poly(ethylene glycol) (M_n = 3000 $g \cdot mol^{-1}$) were purchased from Sigma-Aldrich. Trisodium citrate (99.8%) was purchased from Acros Organics. Ultrahigh quality water with a resistance of 18.2 MΩ.cm (at 25 °C) was obtained from a Millipore Milli-Q gradient machine fitted with a 0.22 μm filter. Preformulated, powdered, phosphate buffered saline was purchased from Sigma-Aldrich, and the desired solution made by addition of ultra high quality water to give [NaCl] = 0.138 M, [KCl] = 0.0027 M, and pH = 7.4. The pH of this solution was adjusted by addition of aqueous 0.1 M HCl or NaOH as needed. All other chemicals were used as received unless otherwise indicated. Dulbecco's Modified Eagle's Medium, PC and M199 medium with and without 10% fetal calf serum were kind gifts from Dr. Ronald Unger, Johannes Gutenberg University, Mainz, Germany. DMEM and M199 were prepared using standard formulations[31,32] and did not contain antibiotics. PC (endothelial cell growth medium) was obtained from Promocell (C-22210) with no additional growth factors or antibiotics added.

Physical and Analytical Methods. The pH of the buffer solutions was measured using a precalibrated pH electrode from Mettler Toledo. UV−vis absorbance spectra were obtained on a Varian Cary 100 Bio spectrophotometer operating at 25 °C using 10 mm path length cuvettes with a total volume of 2.5 mL. Alternatively, UV−vis absorbance spectra were collected using a Tecan Infinite 200 microplate reader using 96-well plates. The method of Fernig and co-workers was used to estimate the diameter of citrate-stabilized gold nanoparticle using UV−vis spectroscopy.[33] X-ray photoelectron spectroscopy (XPS) was carried out on an Axis Ultra instrument from Kratos Analytical. Samples were prepared by adding a small droplet (<0.2 mL) of a 0.1 $mg \cdot mL^{-1}$ aqueous solution of gold nanoparticles onto a silicon wafer and evaporation of the water under a flow of nitrogen, which itself was passed through a 0.2 μm filter. Atomic ratios were calculated taking into account the relative atomic sensitivity factors. Dynamic light scattering measurements were carried out on a Brookhaven Instruments Corporation system consisting of a BI-200SM goniometer and a BI-9000AT autocorrelator. A 100 mW Ar + ion laser (Lexel Lasers) operating at 488 nm was used. All measurements were performed at a temperature of 25.0 (±0.2) °C and at a scattering angle of 90°. Borosilicate cuvettes were used with a minimum of 3 mL of the nanoparticle solution. The nanoparticles were used at a concentration of ∼0.05 $mg \cdot mL$ (total gold mass) in Milli-Q water and passed through a 0.4 μm filter before measurement. Hydrodynamic radii were determined by the CONTIN algorithm using the manufacturer's software. The values quoted are an average from a minimum of 15 experiments. Transmission electron micrographs were obtained using a Phillips CM 20 instrument equipped with a LaB_6 source operated at 200 kV accelerating voltage. Samples were prepared by applying a small (<0.1 mL) amount of a 0.01 $mg \cdot mL^{-1}$ aqueous solution to a copper grid. The excess solution was then removed by swabbing with filter paper, following by drying with an infrared lamp.

PROCEDURES

Synthesis of Citrate-Stabilized Gold Nanoparticles. As a typical example, the synthesis of 12 nm diameter gold nanoparticles is described. First, 350 mL of a 0.83 $mmol \cdot L^{-1}$ (0.33 $mg \cdot mL^{-1}$) aqueous solution of $HAuCl_4$ was heated to reflux in a scratch-free round bottomed flask. After that, 8.57 mL of a 0.1 $mol \cdot L^{-1}$ aqueous solution of sodium citrate was added in a single portion to the $HAuCl_4$ solution to give an Au/citrate ratio 1:3.5. The temperature was maintained at reflux for 30 min, during which time a deep red coloration formed. The reaction mixture was then allowed to cool to room temperature over a period of 3 h. Gold nanoparticles with diameters of 28 and 51 nm were prepared using the same protocol but by adjusting the concentration of the sodium citrate solution to the yield

Scheme 1

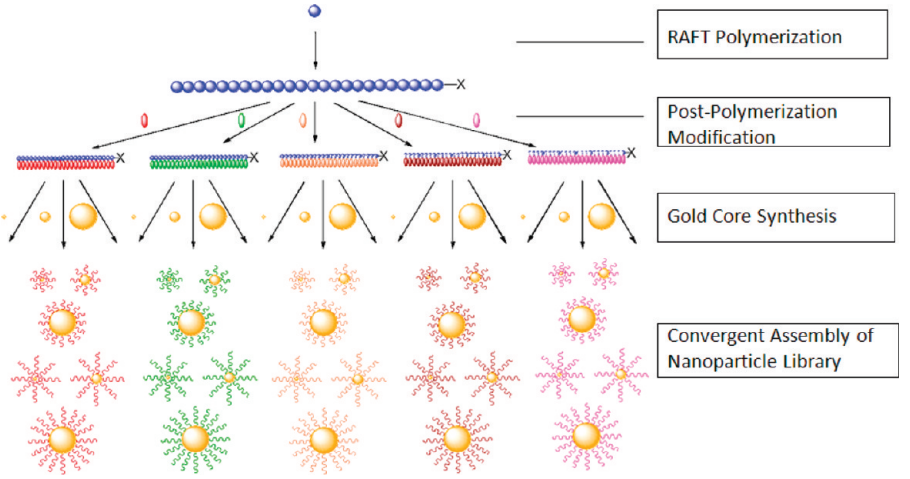

Au/Citrate ratios of 1:2 and 1:1, respectively. Assuming complete reduction of the $HAuCl_4$ into the particles, the total gold concentration in the final solution was 0.83 mmol·L^{-1} (0.16 mg·mL^{-1}).

Synthesis of Thiol-Terminated Polymer Library. The polymer library was synthesized by post-polymerization modification of poly(pentafluorophenyl methacrylate) following previously published protocols.[34] Details of the synthetic and characterization procedures are included in the Supporting Information.

General Procedure for the Synthesis of Polymer-Coated Gold Nanoparticles. Approximately 3 mg of the desired thiol-terminated polymer was added to a falcon tube and dissolved in 0.5 mL of high-purity water. To this tube was added 12 mL of the citrate-stabilized gold nanoparticle solution (0.83 mmol·L^{-1} total gold concentration), which was then agitated overnight in the absence of light. To remove excess polymer, the particles were centrifuged for 3 h at 8000 rpm. Following careful decantation of the supernatant, the particles were then redispersed in 10 mL of high-quality water and the centrifugation-resuspension process repeated for a total of 3 cycles. After the final cycle, the particles were dispersed in 2 mL of high-quality water for future use. Assuming complete incorporation of the citrate coated gold particles into the final polymer coated particles the total concentration of gold in the final solution was 5.0 mmol·L^{-1}, 0.98 mg·mL^{-1}.

Modifications to the General Procedure for the Synthesis of Polymer-Coated Gold Nanoparticles. Polymers $\mathbf{A_{55}}$, $\mathbf{A_{91}}$, $\mathbf{A_{146}}$, $\mathbf{C_{55}}$, $\mathbf{C_{91}}$, and $\mathbf{C_{146}}$ were prepared as aqueous solutions with the pH adjusted to ~5 using 0.01 M $HCl_{(aq)}$ before addition of the citrate-stabilized gold nanoparticle solution. Polymers $\mathbf{E_{55}}$, $\mathbf{E_{91}}$, and $\mathbf{E_{146}}$ were prepared as aqueous solutions with the pH adjusted to ~10 using 0.01 M $NaOH_{(aq)}$ before addition of the citrate-stabilized gold nanoparticle solution.

High-Throughput Aggregation Assays. All assays were conducted in 96-well plates. Solutions were transferred using pipettes with a fresh tip for each nanoparticle type. First, 150 μL of the appropriate buffer, medium or saline solution was added to each well on the plate. Then, 50 μL of a 0.8 mg·mL^{-1} solution of the polymer-coated gold nanoparticles were pipetted into the wells. The plates were gently agitated, then covered and left at room temperature for 1 h. Following this time, UV−visible absorption spectra were recorded using the plate reader and a digital image obtained on a flat-bed scanner. The absorption at the required wavelength (520, 530, or 540 nm for the 12, 28, or 51 nm diameter particles, respectively) was measured and the background of the pure solvent subtracted. To create the visualizations (heatmaps), Heatmap builder Version 1.0 (Freely available from Stanford University, http://mozart.stanford.edu/heatmap.htm) was used.

Determination of Grafting Density of Polymer Chains on Gold Nanoparticles using XPS. The ratio of Au/N for the nanoparticles deposited on a silicon wafer was measured. Taking into account the degree of side-chain functionality (f) of the polymers (Table S1 in the Supporting Information), the degree of polymerization (DP) of the tethered polymers and the diameter of the gold core of the particles ($2r$) the grafting density (Γ) could be calculated using eqs 1−3:

$$N_{Au} = \frac{\pi}{6}\frac{\rho D^3}{M} \quad (1)$$

$$N_{pol} = \frac{I_N}{I_{Au}} * N_{Au} * \frac{f}{\overline{DP}} \quad (2)$$

$$\Gamma = N_{pol}/4\pi r^2 \quad (3)$$

N_{Au} = Gold atoms per sphere; ρ = density of FCC Au = 19.3 g·cm^{-3}; M = atomic weight Au = 196.97 g·mol^{-1}; D = diameter; N_{pol} = number of polymer chains per sphere; I_N/I_{Au} = ratio of the integrals of these atoms in XPS spectra; f = degree of functionalization of polymer side chains; DP = number average degree of polymerization; Γ = grafting density in chains·nm^{-2}.

RESULTS AND DISCUSSION

Nanoparticle Synthesis and Characterization. The polymer-coated gold nanoparticles discussed in this contribution have been prepared following a novel convergent strategy, which is outlined in Scheme 1. The key feature of this strategy is the synthesis of a chemically diverse, thiol end-functionalized polymer library via postpolymerization modification of well-defined polymeric active ester scaffolds, prepared by RAFT polymerization. Compared to direct polymerization of the appropriate functional monomers, post-polymerization modification accelerates synthesis, reduces

Scheme 2[a]

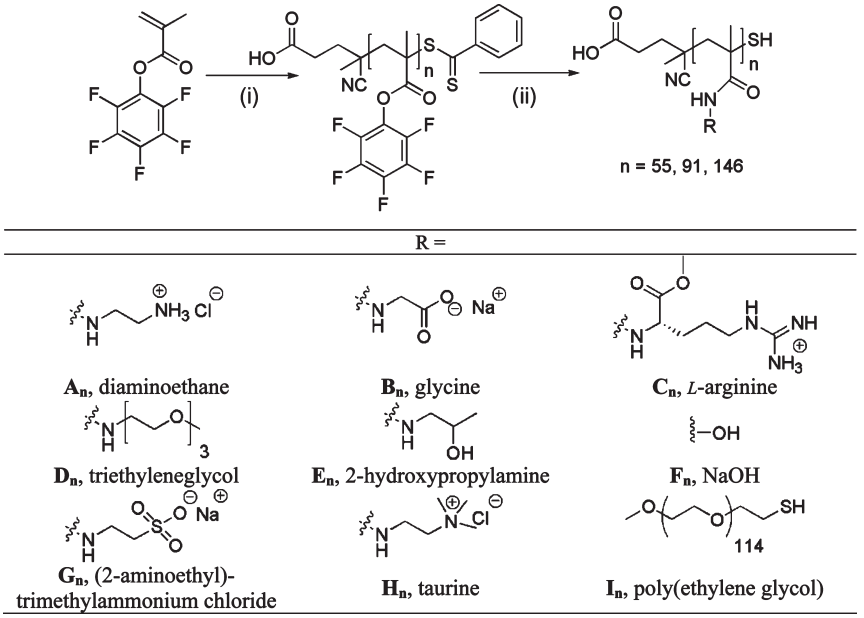

[a] Reaction conditions: (i) CTA and initiator, dioxane, 90 °C; (ii) 2 equivalents of R-NH_2/NEt_3, DMF, 50 °C, 16 h. I_n is linear, thiol-terminated, poly(ethylene glycol), not a poly(methacrylamide).

the total number of characterization steps (e.g., the determination of polymer chain length) and ensures chain length homogeneity across a series. After post-polymerization modification, the resulting thiol end-functionalized polymers are tethered to the surface of the preformed gold particles by a thiol-gold bond to create a diverse library of nanoparticles with predictable size and surface functionality.

The polymers chosen in this study for the surface modification of the gold nanoparticles are side-chain functional, ω-thiol polymethacrylamides, which are prepared as shown in Scheme 2. Full details of the synthesis and characterization of these polymers have been described in a previous publication and the most important data pertinent to this report are included in Table S1 in the Supporting Information.[34] In brief, the synthetic process starts with the RAFT polymerization of pentafluorophenyl methacrylate, followed by addition of a variety of primary amines to replace the pentafluorophenyl ester groups and produce the corresponding polymethacrylamides. In this way, starting with three poly(pentafluorophenyl methacrylate) precursors with degrees of polymerization of 55, 91, and 146 a total of 24 side-chain functional polymethacrylamides was obtained. The RAFT agent used in the synthesis of poly(pentafluorophenyl methacrylate) generates dithiobenzoate chain ends, which are quantitatively cleaved during the postpolymerization modification reaction to give the ω-thiol end-groups.

Three master batches of gold nanoparticle cores with different sizes were prepared by the well-known citrate reduction method.[35,36] The use of only three master batches of gold nanoparticles for the preparation of the polymer-coated particles prevents potential problems due to e.g. different particle size distributions, if particles from different batches were used for a given particle size. The size of the resulting citrate-stabilized nanoparticles was determined by UV−vis spectroscopy and dynamic light scattering (DLS). As shown in Table 1, the results from the UV−vis spectroscopy experiments are in good

Table 1. Particle Sizes of the Gold Core Master Batches Used for the Preparation of the Polymer-Coated Nanoparticles

	particle		
	Au_{12}	Au_{28}	Au_{51}
citrate/Au ratio [a]	3.5:1	2:1	1:1
UV_{Max} (nm)	518	531	536
core diameter UV (nm) [b]	22	40	62
core diameter DLS (nm) [c]	18	45	64
core diameter TEM I_{114} (nm) [d]	11.5 ± 1.8	27.8 ± 11	50.8 ± 13
core diameter TEM B_{91}(nm) [e]	12.2 ± 1.9	26.3 ± 10	50.2 ± 18

[a] Ratio of reactants used during the synthesis of citrate-stabilized nanoparticles. [b] Estimated diameter of the citrate-stabilized particles from UV−vis spectroscopy. [c] Diameter of the citrate-stabilized particles determined from dynamic light scattering. [d] Number-average particle size from a random set of over 30 particles, which were coated with polymer I_{114}. [e] Number-average particle size from a random set of over 30 particles, which were coated with polymer B_{91}.

agreement with the data obtained from DLS and indicate that the diameter of the gold nanoparticles can be varied from ~20 to ~60 nm by decreasing the citrate to gold ratio from 3.5: 1 to 1: 1. In addition to the UV−vis and DLS data, Table 1 also lists particle diameters that were obtained from transmission electron microscopy (TEM) analysis of two series of particles, which were modified with polymers I_{114} and B_{91}, respectively (vide infra). There was no significant difference in the TEM diameter between the two coatings used. The particle sizes obtained by TEM were slightly smaller than the values obtained by UV−vis and DLS analysis. These differences can be attributed to TEM measuring only the gold particle core in the dry state, whereas DLS gives the hydrodynamic diameter, including the citrate shell, of the particle in the dispersed state. There was no increase in diameter, which could be associated with aggregation or further

dx.doi.org/10.1021/co100099r |ACS Comb. Sci. 2011, 13, 286–297

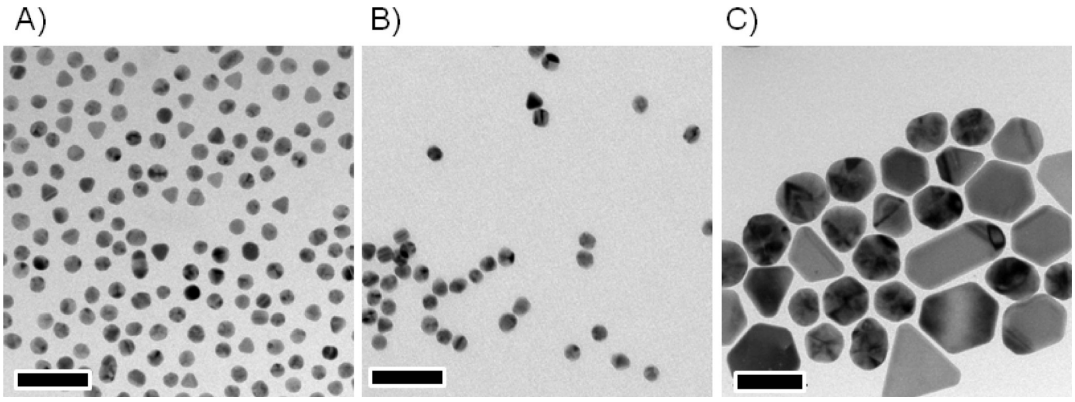

Figure 1. TEM images of polymer-coated gold nanoparticles. (a) $\mathbf{I_{114}@Au_{12}}$; (b) $\mathbf{B_{91}@Au_{12}}$; (c) $\mathbf{I_{114}@Au_{51}}$. Scale bar =50 nm.

particle growth, highlighting the mild functionalization method of thiol-gold attraction. In addition to size, the TEM experiments also provide information on the morphology of the gold nanoparticles. The images, which are shown in Figure 1, indicate an increased population of irregular shaped particles with decreasing citrate/gold ratios, that is, with increasing particle size. Nonetheless, there were still more spherical-like particles than angular shaped even for the largest particle size (51 nm). Throughout the remainder of this manuscript, the gold nanoparticles will be referred to as $\mathbf{Au_{12}}$, $\mathbf{Au_{28}}$, or $\mathbf{Au_{51}}$, where the subscript indicates the particle diameter as determined by TEM.

The polymer-coated gold nanoparticles were prepared by mixing aqueous solutions of the desired gold nanoparticle with the appropriate polymer and subsequent agitation overnight under the exclusion of light. Using the three different gold nanoparticle batches discussed above and 25 different thiol end-functionalized polymers, a 75 member polymer-coated gold nanoparticle library was generated (Table 2). It should be noted here that in contrast to polymers **A**−**H**, polymer $\mathbf{I_{114}}$ is not a polymethacrylamide but a commercially available, thiol-terminated poly(ethylene glycol). Polymers $\mathbf{A}_n$ and $\mathbf{C}_n$ can potentially interact with the citrate-stabilized gold nanoparticles through both their side chains as well as via the terminal thiol group. Indeed, when these polymers and citrate-stabilized gold nanoparticle solutions are mixed together, the color rapidly changes from red to blue indicating aggregation. This problem was circumvented by lowering the pH to ∼5, which results in protonation of the side-chain functional groups, reducing their affinity for the gold surface. Under these conditions, however, electrostatic deposition of the polycations onto the citrate-stabilized surface is a potential side reaction. While this cannot completely be ruled out here, the DLS data shown in Figure 2 and discussed below (vide infra) suggest that the polymers are tethered by their chain ends and that no aggregation due to bridging flocculation occurred. In some cases, polymers $\mathbf{E}_n$ led to aggregation, particularly when the particle core size was above 50 nm. This could be prevented by increasing the pH to 10. In keeping with the high-throughput philosophy of this nanoparticle library synthesis method, purification to remove excess polymer and citrate ligands was achieved by simple centrifugation-resuspension cycles. This purification method has been used extensively in the literature,[19,25,26] and the separation of the gold nanoparticles from solution can be conveniently monitored by either UV−vis spectroscopy or simple visual observations of the supernatant, due to the reduction in the deep red color associated with gold nanoparticle dispersions. The resulting particles could be dissolved in good solvents for the polymers (e.g., $CHCl_3$ for coating $\mathbf{D}_n$ and MeOH for $\mathbf{E}_n$) also suggesting that successful modification had occurred.

Following removal of the excess polymer, UV−vis spectra were collected for the whole nanoparticle library. The location of the surface plasmon resonance (SPR) band for each of the polymer-coated gold nanoparticles is listed in Table 2. The SPR peak location of the polymer-coated particles is shifted compared to the citrate-stabilized particles, which reflects the changes in the local refractive index due to the polymer surface modification. The changes in the SPR location were relatively small (typically <10 nm) also effectively ruling out interparticle aggregation, which would have resulted in much larger shifts (>100 nm).[37] For several series of particles, especially those based on the two largest gold cores, SPR peak maxima were found to shift to slightly shorter wavelengths with increasing degree of polymerization of the grafted polymer. For a given polymer at a fixed degree of polymerization, increasing the gold core diameter generally results in a blue shift of the SPR band. It is difficult to draw any more detailed conclusions as the particles do not only differ with respect to the degree of polymerization of the grafted polymer and the gold core size, but also have different surface chemistries and grafting densities. When the aqueous solutions containing the polymer-coated gold nanoparticles were investigated again with UV−vis spectroscopy after storing for 14 days, the location of the SPR peak was the same (±3 nm) as directly after synthesis and purification (Figure S1, Supporting Information). This indicates that the polymer-coated gold nanoparticles were stable to aggregation in water for at least two weeks. To further probe the functionalization reaction and to characterize the polymer-coated particles, the library was analyzed by DLS in aqueous solution. Figure 2 shows the results of this analysis and illustrates that the gold nanoparticle size determines the final hydrodynamic diameter. For all particles, the measured hydrodynamic diameters are larger than that of the corresponding gold core, confirming that the surface has been modified with the polymers. Across the whole library, particles with identical core sizes and chemical functionality displayed slightly increased particle sizes as the polymer chain length was increased. For a given gold core diameter, different chemical coatings of identical polymer chain length, however, showed some variation in particle diameter. These variations can be attributed to: (1) attractive or repulsive intra- and interchain interactions leading to an extension or collapse of the surface

Table 2. Overview of the Polymer-Coated Nanoparticle Library Prepared and Investigated in This Study

Particle Core	Au_{12}		Au_{28}		Au_{51}	
R =	Code[a]	UV_{Max}[b]	Code[a]	UV_{Max}[b]	Code[a]	UV_{Max}[b]
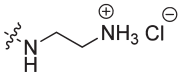 Ethane diamine (**A**)	$A_{55}@Au_{12}$	527	$A_{55}@Au_{28}$	532	$A_{55}@Au_{51}$	539
	$A_{91}@Au_{12}$	526	$A_{91}@Au_{28}$	533	$A_{91}@Au_{51}$	539
	$A_{146}@Au_{12}$	528	$A_{146}@Au_{28}$	529	$A_{146}@Au_{51}$	538
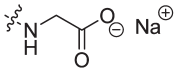 Glycine (**B**)	$B_{55}@Au_{12}$	527	$B_{55}@Au_{28}$	531	$B_{55}@Au_{51}$	544
	$B_{91}@Au_{12}$	527	$B_{91}@Au_{28}$	529	$B_{91}@Au_{51}$	546
	$B_{146}@Au_{12}$	523	$B_{146}@Au_{28}$	528	$B_{146}@Au_{51}$	538
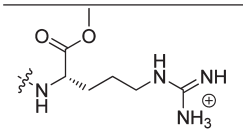 L-Arginine methyl ester (**C**)	$C_{55}@Au_{12}$	527	$C_{55}@Au_{28}$	532	$C_{55}@Au_{51}$	539
	$C_{91}@Au_{12}$	527	$C_{91}@Au_{28}$	531	$C_{91}@Au_{51}$	540
	$C_{146}@Au_{12}$	528	$C_{146}@Au_{28}$	532	$C_{146}@Au_{51}$	539
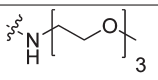 PEG_3-NH_2 (**D**)	$D_{55}@Au_{12}$	525	$D_{55}@Au_{28}$	531	$D_{55}@Au_{51}$	539
	$D_{91}@Au_{12}$	526	$D_{91}@Au_{28}$	530	$D_{91}@Au_{51}$	540
	$D_{146}@Au_{12}$	526	$D_{146}@Au_{28}$	529	$D_{146}@Au_{51}$	539
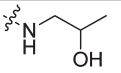 Hydroxypropylamine (**E**)	$E_{55}@Au_{12}$	527	$E_{55}@Au_{28}$	531	$E_{55}@Au_{51}$	560
	$E_{91}@Au_{12}$	525	$E_{91}@Au_{28}$	532	$E_{91}@Au_{51}$	545
	$E_{146}@Au_{12}$	524	$E_{146}@Au_{28}$	531	$E_{146}@Au_{51}$	561
 (**F**)	$F_{55}@Au_{12}$	522	$F_{55}@Au_{28}$	530	$F_{55}@Au_{51}$	538
	$F_{91}@Au_{12}$	523	$F_{91}@Au_{28}$	527	$F_{91}@Au_{51}$	536
	$F_{146}@Au_{12}$	527	$F_{146}@Au_{28}$	528	$F_{146}@Au_{51}$	538
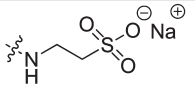 Taurine (**G**)	$G@Au_{12}$	516	$G_{55}@Au_{28}$	528	$G_{55}@Au_{51}$	537
	$G_{91}@Au_{12}$	516	$G_{91}@Au_{28}$	528	$G_{91}@Au_{51}$	535
	$G_{146}@Au_{12}$	516	$G_{146}@Au_{28}$	528	$G_{146}@Au_{51}$	536
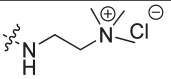 (2-Aminoethyl)trimethyl-ammoniumchloride (**H**)	$H_{55}@Au_{12}$	526	$H_{55}@Au_{28}$	531	$H_{55}@Au_{51}$	538
	$H_{91}@Au_{12}$	523	$H_{91}@Au_{28}$	531	$H_{91}@Au_{51}$	537
	$H_{146}@Au_{12}$	524	$H_{146}@Au_{28}$	530	$H_{146}@Au_{51}$	537
PEG_{114}-SH (**I**)	$I_{114}@Au_{12}$	526	$I_{114}@Au_{28}$	533	$I_{114}@Au_{51}$	538

[a] Particle labels: $X_n@Au_m$ X = polymer coating used; *n* = degree of polymerization of the polymer coating; *m* = diameter of gold nanoparticle (in nm) as determined by TEM. [b] Wavelength of maximum absorption (SPR peak) of solution of polymer-coated particles in aqueous solution measured using a total gold concentration ~0.05 mg·mL^{-1}.

grafted polymer chains and (2) variation of grafting density. Within a given gold core size, the variation of hydrodynamic diameters of the corresponding polymer-coated particles was only 10 nm for the smallest gold cores and 20 nm for the largest, which rules out aggregation. The DLS data in Figure 2, in addition to the UV−vis data, also further confirm that the final particles are modified with the polymers and that it is possible to control the diameter of these particles even with a huge variety of different functional groups incorporated into the coatings.

To determine the grafting density of polymer chains on gold nanoparticles, thermogravimetric analysis is commonly used. For high-throughput synthesis, this method requires a relatively large quantity of material, so X-ray photoelectron spectroscopy (XPS) was used instead. XPS was only used to analyze the smallest particles as the penetration depth of the X-rays, ~10 nm, is similar to the diameter of the 12 nm gold particles (Supporting Information).[38] The atomic ratio of gold to nitrogen can then be used to estimate the grafting density and compare the effects of different chemistries and polymer chain lengths. The key assumption here is that the particles are spheres with face-centered cubic (FCC) packing of gold atoms and that the X-rays penetrate the whole particle and the coating. The ratio of Au/N was measured (as only the polymers contain nitrogen) and taking into account the degree of side chain functionality (*f*) of the polymer (Table S1 in the Supporting Information), polymer chain length and the diameter of the particles, the grafting density could be calculated. Details of the calculation are given in the Experimental Procedures and the results for selected particles are presented in Table 3. The grafting densities listed in Table 3 are in good agreement with those obtained for other thiol-terminated polymers, as summarized by Shan and Tenhu, which were in the range of 0.32 − 2.86 chains.nm^{-2}.[13] For all the

dx.doi.org/10.1021/co100099r |*ACS Comb. Sci.* 2011, 13, 286–297

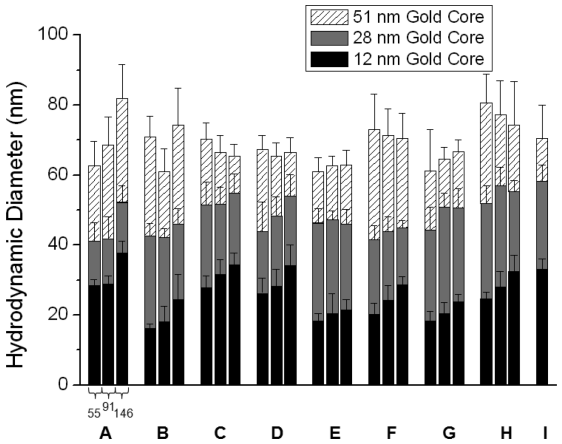

Figure 2. DLS analysis of the polymer-coated nanoparticle library obtained in water with a total gold concentration of ~0.025 mg·mL^{-1}. The degree of polymerization of the polymer coating used is indicated below the bars of the *x*-axis. The same labeling is used along the series, as exemplified for **A**. **I** has DP = 114. Scale bars represent standard deviation and only the positive bars are shown for clarity.

Table 3. XPS Analysis and Calculated Grafting Densities for Selected Polymer-Coated Particles

particle	atomic ratio (I_N/I_{Au}) [a]	grafting density (chains·sphere^{-1}) [b]	grafting density (chains·nm^{-2}) [b]
$\mathbf{A_{55}@Au_{12}}$	1.05	511	1.13
$\mathbf{A_{91}@Au_{12}}$	0.44	130	0.29
$\mathbf{A_{146}@Au_{12}}$	0.73	133	0.29
$\mathbf{B_{55}@Au_{12}}$	0.28	584	1.29
$\mathbf{B_{91}@Au_{12}}$	0.32	396	0.87
$\mathbf{B_{146}@Au_{12}}$	0.16	119	0.26
$\mathbf{D_{55}@Au_{12}}$	0.37	493	1.09
$\mathbf{D_{91}@Au_{12}}$	0.33	264	0.58
$\mathbf{D_{146}@Au_{12}}$	0.57	264	0.58

[a] I_N = Integral of the XPS signal arising from nitrogen atoms; I_{Au} = Integral of the XPS signal arising from gold atoms. [b] Assuming the X-rays penetrate the whole particle and that the particles are perfect spheres.

polymer-coated particles that were studied with XPS, those with the shortest chain length (DP = 55) showed the highest grafting density, which would be expected from steric considerations. The grafting density decreased as the polymer chain length increased. For polymers with DP = 146, coating **D** gave higher grafting densities than **A** or **B**. Although **D** has a rather large triethylene glycol side chain, it is neutral, unlike **A** and **B**, which are charged and thus experience not only steric crowding but also electrostatic repulsion. The close agreement with literature values suggests that the calculated grafting densities, which are in the range of 0.26−1.29 chains·nm^{-2} are reasonable. As the escape depth of the photoelectrons is similar to the size of the gold nanoparticle cores, however, the grafting densities may be slightly overestimated.[39]

To further probe the functionalization of the gold nanoparticles, zeta potential measurements were conducted. For these experiments, several particles, which were coated with poly(2-hydroxypropyl methacrylamide) (polymers $\mathbf{E_{55}}$, $\mathbf{E_{91}}$ and $\mathbf{E_{146}}$) were selected as shown in Table 4. A neutral polymer was chosen

Table 4. Zeta Potential Analysis of Selected Nanoparticles

citrate-coated nanoparticle core	ζ (mV)[a]	polymer-coated nanoparticle	ζ (mV)[b]
		$\mathbf{E_{55}@Au_{12}}$	−6.4 ± 2.3
$\mathbf{Au_{12}}$	−24.1 ± 10.8	$\mathbf{E_{91}@Au_{12}}$	−3.9 ± 5.5
		$\mathbf{E_{146}@Au_{12}}$	−17.2 ± 3.1
		$\mathbf{E_{55}@Au_{28}}$	−10.9 ± 3.0
$\mathbf{Au_{28}}$	−23.2 ± 9.6	$\mathbf{E_{91}@Au_{28}}$	−14.6 ± 4.3
		$\mathbf{E_{146}@Au_{28}}$	−6.9 ± 7.7
		$\mathbf{E_{55}@Au_{51}}$	−12.9 ± 8.5
$\mathbf{Au_{51}}$	−25.1 ± 10.2	$\mathbf{E_{91}@Au_{51}}$	−10.9 ± 3.2
		$\mathbf{E_{146}@Au_{51}}$	−6.2 ± 9.3

[a] Obtained in 10 mM phosphate buffered saline at pH 7.4. Total gold concentration = 0.05 mg.mL^{-1}. Aggregation occurred because of instability of citrate coated particles in salt solutions, which may affect data. [b] Obtained in 7.5 mM $NaNO_3$ at pH 7.2. Total gold concentration = 0.05 mg.mL^{-1}. Errors represent standard deviation.

as this will not contribute to the net charge of the particle therefore allowing the change in zeta potential upon addition of the polymers to be investigated. The citrate-coated particles tended to aggregate in all buffers (vide infra), and the best data was obtained in phosphate buffered saline. These results are included in Table 4, but because of the aggregation during the measurements they have significant error. Literature values for the zeta potential of citrate coated gold nanoparticles are in the range of −29 to −50 mV indicating that the values obtained here (~−25 mV) might be underestimates of the magnitude.[40] Zeta potentials of the $\mathbf{E_{56}}$, $\mathbf{E_{91}}$, and $\mathbf{E_{146}}$ coated particles were determined in 7.5 mM $NaNO_3$ at pH 7.2 and determined by Henry's approximation.[41] Under these conditions, UV−vis spectroscopy indicated that the particles were not aggregated. The results in Table 4 clearly show that the zeta potential becomes less negative (i.e., approaches zero) following addition of the polymer coating indicating successful surface modification. Within the error of the measurements as indicated in Table 4, these data are in reasonable agreement with results by Davis et al., who also recently reported that modification of citrate-stabilized gold nanoparticles with trithiocarbonate end functionalized poly(oligo(ethylene glycol)acrylate) or poly((diethylene glycol)acrylate) resulted in hybrid nanoparticles with a slightly negative residual zeta potential.[42] The data in Table 4 reveal no general trend between the final zeta potential and either particle core size or the degree of polymerization of the polymer chain. For the 12 nm particles, addition of polymer with DP = 55 gave a less negative zeta potential compared to a polymer with a DP = 146, suggesting larger polymers do not coat the particles as efficiently as smaller ones. However, with 51 nm particles the opposite trend is observed. These differences may be due to the error associated with the measurements or represent a different trend regarding the availability of surface sites of gold nanoparticles for polymer binding or the degree of curvature for different sizes of nanoparticles. The overall net negative charge of the particles suggests that there is some residual citrate present. Analysis of the XPS spectra of several particles reveals the presence of a sodium peak (Na 2s) at 62.8 eV from residual sodium citrate. While the presence of residual citrate is an important consideration in the application of these nanoparticles, it should be noted that this is a common issue for most gold nanoparticle based materials and should not limit the application of this new library-based approach.

Nanoparticle Aggregation. Well-defined nanoparticle libraries that cover a range of particle sizes and with diverse surface chemistry are attractive tools to study, for example, nanoparticle toxicity, cell uptake, or trafficking. The biological properties of nanoparticles, however, are not necessarily only determined by particle size and surface chemistry, but can also be influenced by particle aggregation. As a consequence, knowledge about the aggregation properties of nanoparticles and an understanding of the fundamental structure−property relationships that underlie these phenomena prior to their use in any biological study is very important. The objective of the second part of this manuscript was to systematically study the aggregation behavior of the nanoparticle libraries discussed in the first section. The gold core of the nanoparticles presented here greatly facilitates these studies, since the SPR band of the gold core shifts to longer wavelengths during aggregation because of interparticle coupling effects resulting in a shift in color from red to blue.[10,37] The experiments discussed in this section were carried out in 3 different media: saline solution, phosphate buffered saline and cell culture medium. As an example, Figure 3 shows UV−vis spectra of $\mathbf{A_{91}@Au_{12}}$ recorded in saline solutions with different NaCl concentrations. There is a clear reduction in the absorbance at 525 nm and the location of the SPR peak shifts to longer wavelength as [NaCl] increases allowing observation of the aggregation process. To aid in the evaluation of aggregation of the nanoparticle library, a high-throughput technique was developed using 96-well microplates and a microplate reader, which have also been used by Brust and Cooper to aid in the design of gold nanoparticle stabilizing ligands.[26,43] The experiments were carried out by adding the gold nanoparticles to the desired solutions to give a total gold concentration of 0.2 mg·mL^{-1}.

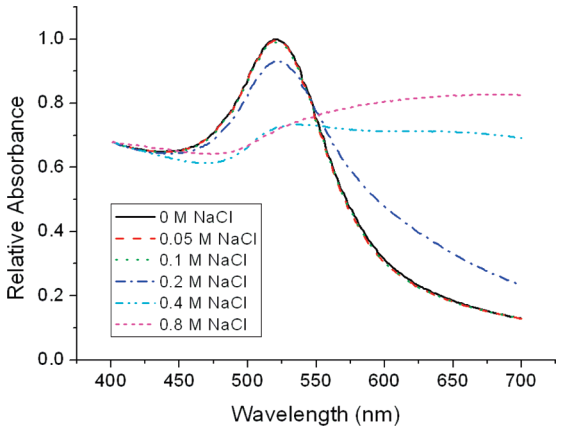

Figure 3. UV−vis absorption spectra of $\mathbf{A_{91}@Au_{12}}$ recorded in saline solutions with different [NaCl]. The values are scaled such that 0 M NaCl has an absorbance value of 1 at 520 nm. [Au NP] = 0.2 mg·mL^{-1}.

The resulting nanoparticle solutions were analyzed after an incubation time of 1 h. Figure 4 shows an image, which was obtained using a flatbed scanner, of selected nanoparticles in saline solutions with different [NaCl]. For the $\mathbf{Au_{12}}$ based particles, the color of the dispersion changes from red to blue to transparent/gray (the color appears as gray due to the background during scanning of the image) as the NaCl concentration of the saline solution increases, indicating particle aggregation at high NaCl concentrations. Unfortunately, the $\mathbf{Au_{51}}$ based particles, which according to the DLS data in Figure 2 do not aggregate under salt-free conditions, already display a relatively dark color in their freely dispersed state ([NaCl] = 0 M). As a consequence visual, colorimetric evaluation of the nanoparticle dispersions is not an appropriate strategy to investigate aggregation behavior and alternative approaches are needed.

Instead of colorimetric evaluation, another method to assess the aggregation stability of the polymer-coated nanoparticle library is to spectrophotometrically monitor the change in the intensity at or near the SPR peak. For these experiments, the use of 96-well plates is more convenient than using individual UV cuvettes or dynamic light scattering experiments and requires less material per experiment. The measurements were acquired at 520, 530, or 540 nm for the 12, 18, and 51 nm nanoparticles, respectively. In Figures 5−7 the relative aggregation of the nanoparticles is presented as heatmaps. The degree of aggregation is expressed as the relative change in the absorbance at the SPR peak of the nanoparticle solutions, compared to a reference sample. The data was normalized, such that the reference value was equal to 1 and the decrease (or increase) in the absorbance relative to this was plotted. In all the heatmaps, the reference value is the first vertical column for each nanoparticle size. In Figure 5, the influence of salt concentration is investigated, relative to pure water, which was set as the reference and has a value of 1. In Figures 5−7, red represents more dispersed particles and green more aggregated. Figure 5 indicates that the citrate-stabilized gold particles aggregate at the lowest NaCl concentration used, 0.05 M. The other charged particles (coatings **A**, **B**, **C**, **F**, **G**, **H**) also display increased aggregation as the salt concentration is increased. As expected, coating the gold nanoparticle cores with a neutral polymer (**D**, **E**, **I**) results in hybrid nanoparticles that are much less sensitive toward aggregation at increasing salt concentration. A few of the neutral particles, especially those based on the largest gold cores, show some aggregation behavior at the higher NaCl concentrations, which is in line with the small negative zeta potential that was determined for these particles (vide supra). Surprisingly, particles with coating **B** (glycine) show good stability to aggregation across the whole range, whereas coating **H**, which also has carboxylic acid functionality is less stable. The length of the polymer chain did not have a significant effect on aggregation.

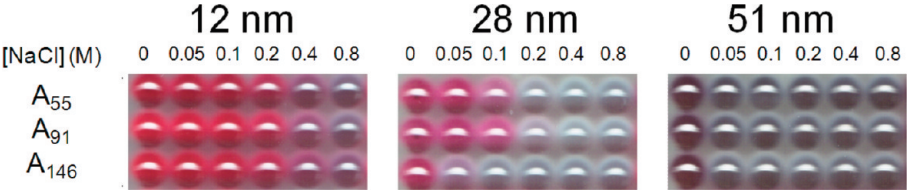

Figure 4. Optical photographs illustrating the effect of increasing salt concentration on the aggregation behavior of selected polymer-coated gold nanoparticles. The images show small sections of 96-well plates containing nanoparticles in NaCl solutions, following 1 h incubation at room temperature.

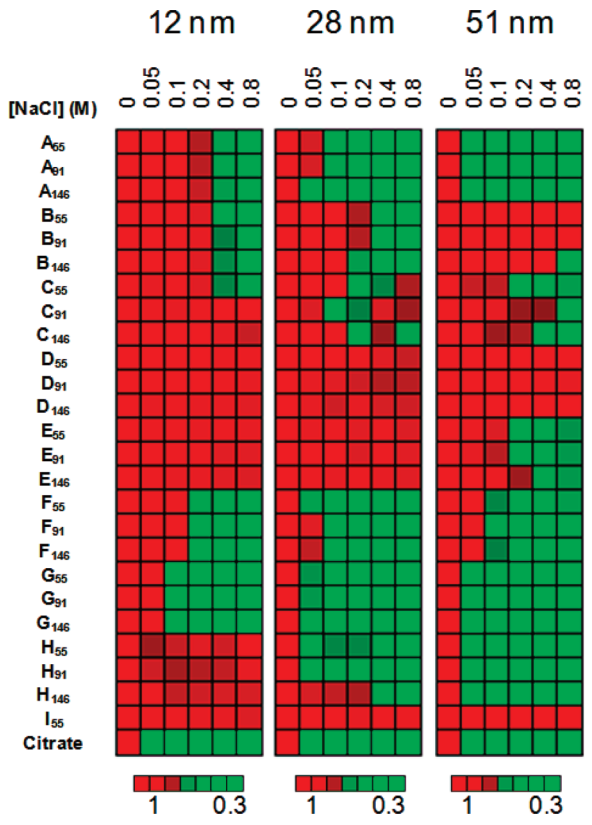

Figure 5. Heat map showing effect of salt concentration on the aggregation stability of the nanoparticle library. [AuNP] = 0.2 mg·mL^{-1}.

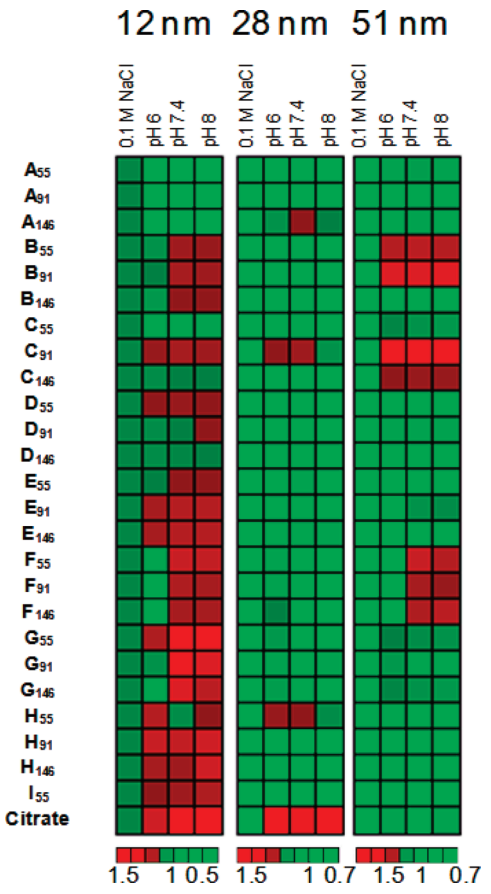

Figure 6. Heat map showing effect of pH in phosphate buffer saline on the aggregation of the nanoparticle library, relative to 0.1 M NaCl solution. [AuNP] = 0.2 mg·mL^{-1}.

The heat map in Figure 6 compares the effect of pH on the aggregation stability of PBS solutions of the polymer coated gold nanoparticles. To evaluate the influence of both the phosphate component and the pH, the reference in these studies was the absorbance of the SPR peak in 0.1 M NaCl. Figure 6 again shows the general trend that the 51 nm core nanoparticles were more aggregated than the 12 or 28 nm nanoparticles under identical conditions. Increasing the pH generally led to less aggregation for the particles with carboxylic acid side chains (**B** and **F**) because of changes in the degree of protonation. However, for both these coatings, the 28 nm particles did not show a significant response to the pH whereas the 12 and 51 nm particles did, indicating some size effects. Coating $\mathbf{C}_n$ showed better aggregation stability than $\mathbf{A}_n$, particularly at higher pH values, when the guanidinium group (pK_a ~12.5) most likely remains protonated to a greater extent than the primary amine (pK_a ~9.5), increasing repulsions between alike particles. The 12 and 51 nm core nanoparticles with coatings **B**, **F**, and **G** (anionic) showed improved aggregation stability in phosphate buffered saline relative to 0.1 M NaCl at all pH's except for coating **F** which was slightly more aggregated at pH 6 compared to 0.1 M NaCl. The 28 nm core nanoparticles with coatings **B**, **F**, and **G** showed smaller changes than the other diameters. A similar trend was observed for the cationic coatings suggesting that the diameter range around 28 nm is less responsive to changes in buffer conditions than the other diameters. The neutral particles either showed a small decrease or no change in the aggregation relative to salt only. There were no clear trends regarding the polymer chain length influence on aggregation.

In a final series of experiments, the aggregation stability of the polymer-coated nanoparticle library in a variety of cell culture media was investigated. For the experiments reported here, three common cell culture media were used: DMEM, M199, and PC, both with and with 10% fetal calf serum (FCS). The results of the experiments are summarized in the heatmap in Figure 7, and the degree of aggregation was determined relative to that in pure water (set to value of 1) shown in the first column for each size range. In Figure 7 the presence of 10% FCS is indicated by a plus sign "+" after the name of the medium. As seen in the other solvent conditions, the neutral polymers (**D**, **E**, **I**) showed no or very small responses to the presence or absence of FCS. This is expected as uncharged, hydrophilic polymers are often employed for the synthesis of surfaces resistant to nonspecific adsorption of proteins.[44] Coating $\mathbf{C}_n$, which has guanidinium side chains, also displays stability to aggregation in the absence of FCS. This is in contrast to the other charged polymers $\mathbf{A}_n$, and to a lesser extent $\mathbf{H}_n$, which aggregate in the absence of FCS. Following addition of FCS, all charged particles (**A**, **B**, **C**, **F**, **G**, **H**) display reduced aggregation, with the exception of $\mathbf{A}_n$, in DMEM. In this medium, even following addition of FCS, aggregation was observed, which implies the specific culture medium also affects aggregation. The negatively charged particles (**B**, **F**, **G**) also displayed less aggregation following addition of FCS, indicating that the soluble proteins influence both positively and negatively charged surfaces. For the previous two solvent conditions (saline and PBS solutions), there appeared to be a strong size-dependency on

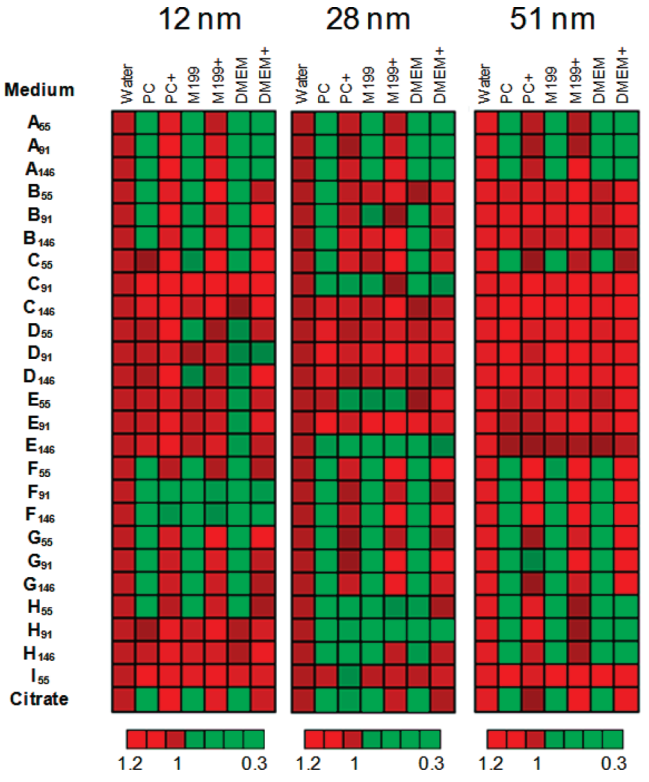

Figure 7. Heat map showing effect of cell culture medium and added serum proteins on nanoparticle aggregation relative to water. [AuNP] = 0.2 mg·mL^{-1}.

the aggregation behavior of the nanoparticles, with the larger particles generally undergoing aggregation to a greater extent than the smaller particles. In the case of the cell culture medium, there is no strong dependence on particle size on the aggregation. This may be due to two factors: First, the change in aggregation state upon addition of the serum proteins was relatively large compared to the other solvent conditions meaning that subtle differences attributable to nanoparticle diameter are harder to observe using the assay developed here. Second, the concentration of dissolved salts, sugars and buffer in the cell culture medium is relatively high such that (in the absence of FCS) all the particles are already aggregated to the same extent which also prevents comparison.

To confirm that the addition of FCS did indeed reduce aggregation, as suggested by the heatmaps in Figure 7, and was not an artifact of the assay protocol, additional DLS experiments were carried out. Figure 8 compares the results of DLS analysis of $\mathbf{A_{55}@Au_{28}}$ in pure water, and in PC medium with and without FCS. DLS analysis of $\mathbf{A_{55}@Au_{28}}$ in water reveals an average diameter of around 40 nm in water. In PC medium, without FCS, the diameter is increased to over 200 nm indicating that aggregation occurred. Finally, in PC medium with FCS, the diameter returns to approximately 50 nm confirming that little or no aggregation is present. The small increase in diameter between the particle in water and PC plus serum, might indicate surface absorption of the protein, but can also be due to the influence of using two different solvents in which the polymer brush on the nanoparticle surface displays different swelling capacity and hence different hydrodynamic volume.

Considering the results from the three different solvent systems (saline, phosphate buffered saline and cell culture media) a general trend can be seen that other than surface functionality,

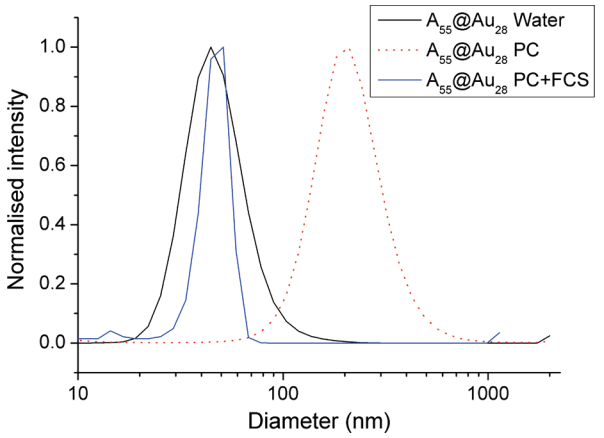

Figure 8. DLS analysis of particle $\mathbf{A_{55}@Au_{28}}$ in water and PC cell culture medium with and without 10% fetal calf serum. Total gold concentration ~0.025 mg·mL^{-1}.

particle size is also a key feature in nanoparticle aggregation. For a given coating chemistry and polymer chain length, the larger particles consistently showed signs of aggregation at lower concentrations of solute than for the smaller particles. This could be due to there being a reduced mass fraction of the polymer coating as the particle core size increases from 12 to 28 to 51 nm. As the polymer coating is expected to control the interaction of the particle with the solvent, changing the relative mass on the particle could have a strong influence on the particle's propensity to aggregate. Varying polymer chain length at a given gold core size and coating chemistry did not appear to significantly influence the aggregation properties for most particles in this study. As can be seen from Table 3, increasing polymer chain length decreases the grafting density and the polymer mass fraction of the particle. On the other hand, longer chains provide more steric hindrance to aggregation, perhaps canceling out the effect of reduced mass fraction. The results presented here cannot completely rule out polymer chain length-dependent aggregation outside of the range used or upon varying the grafting density. The aggregation assays in different solvents clearly show that with the exception of neutral particles, aggregation to some degree occurs in a wide range of biologically relevant solvent conditions. Furthermore, the presence of serum proteins changes the solution behavior of the nanoparticles, thus suggesting that additional control experiments to determine nanoparticle size and aggregation are required for biological investigations in the presence of serum proteins. What should be noted is that some residual citrate is still present on the surface, which will contribute to the aggregation behavior observed, particularly the salt concentration effects to which the citrate-coated nanoparticles are very susceptible to. However, these results will be consistent with other polymer-coated gold nanoparticle systems, prepared by the "grafting to" method. The general trends may also be applicable to other nanoparticle systems, which feature a polymeric corona.

CONCLUSIONS

A new, facile, convergent strategy to create polymer-coated gold nanoparticle libraries has been presented here. Through a simple mixing strategy multifunctional, thiol-terminated polymers, generated by post-polymerization modification of poly(pentafluorophenyl methacrylate), are added to preformed

citrate-stabilized gold nanoparticles. From 3 precursor polymers and 3 nanoparticle cores a total of 75 unique nanoparticles were created with control over both size and functionality, giving particle diameters in the rage of 18−85 nm. No aggregation of the particles occurred during the functionalization process, as determined by TEM, UV, and DLS measurements and all the particles were well-dispersed in aqueous solution for at least 2 weeks. The obtained polymer library had dimensions controlled by the precursor particle size, and surface chemistries determined by the polymer functionality. X-ray photoelectron spectroscopy suggested that the polymer brushes were densely packed with grafting densities in the range of 0.3−1.2 chains·nm^{-2} and thus confirming the presence of surface-tethered polymer chains. The unique optical properties of the gold nanoparticles were then exploited to create a high-throughput test for nanoparticle aggregation. The influence of particle size, polymer chain length and polymer side chain functionality on aggregation in 15 different solvent conditions were evaluated. Larger and charged particles were shown to be more prone to aggregation generally. Interestingly, addition of serum proteins in cell culture medium results in less nanoparticle aggregation compared to the medium alone, suggesting that serum proteins readily absorb onto many nanoparticle surfaces which, in turn is expected to strongly influence their biological behavior and interpretations of biotesting results. This method represents a powerful, yet easily accessible, tool to create novel nanoparticulate systems using established synthetic protocols and may find many further applications as model nanoparticles for biological, biomedical or electronic systems.

■ ASSOCIATED CONTENT

Supporting Information. Details and characterization of the polymer library and example XPS spectra, along with additional experimental information. This material is available free of charge via the Internet at http://pubs.acs.org.

■ AUTHOR INFORMATION

Corresponding Author

*E-mail: harm-anton.klok@epfl.ch. Fax: + 41 21 693 5650.

Present Addresses

†Department of Chemistry, University of Warwick, Coventry, U.K., CV4 7AL

Funding Sources

The EU is acknowledged for providing funding through the integrated project "Nanobiopharmaceutics", NMP4-CT-2006-026723.

■ ACKNOWLEDGMENT

Dr. Ronald Unger (Mainz) and Dr. Eleonore Fröhlich (Graz) are thanked for helpful discussions with regard to nanoparticle aggregation. Danièle Laub is thanked for assistance with acquiring the TEM images and Prof. Heinrich Hofmann for providing access to his ZetaPALS instrument.

■ REFERENCES

(1) Yan, H.; Park, S. H.; Finkelstein, G.; Reif, J. H.; LaBean, T. H. DNA-Templated Self-Assembly of Protein Arrays and Highly Conductive Nanowires. *Science* **2003**, *301*, 1380–1384.

(2) Sun, S.; Murray, C. B.; Weller, D.; Folks, L.; Moser, A. Monodisperse FePt Nanoparticles and Ferromagnetic FePt Nanocrystal Superlattices. *Science* **2000**, *287*, 1989–1992.

(3) De, M.; Ghosh, P. S.; Rotello, V. M. Applications of Nanoparticles in Biology. *Adv. Mater.* **2008**, *20*, 4225–4241.

(4) Nel, A.; Xia, T.; Li, N. Toxic Potential of Materials at the Nanolevel. *Science* **2006**, *311*, 622–628.

(5) Hussain, S. M.; Braydich, Stolle; Schrand, A. M.; Murdock, R. C.; Yu, K. O.; Mattie, D. M.; Schlager, J. J.; Terrones, M. Toxicity Evaluation for Safe Use of Nanomaterials: Recent Achievements and Technical Challenges. *Adv. Mater.* **2009**, *21*, 1549–1559.

(6) Discher, D. E.; Eisenberg, A. Polymer Vesicles. *Science* **2002**, *297*, 967–973.

(7) Sussman, E. M.; Clarke, M. B., Jr.; Shastri, V. P. Single-Step Process to Produce Surface-Functionalized Polymeric Nanoparticles. *Langmuir* **2007**, *23*, 12275–12279.

(8) van der Ende, A. E.; Kravitz, E. J.; Harth, E. Approach to Formation of Multifunctional Polyester Particles in Controlled Nanoscopic Dimensions. *J. Am. Chem. Soc.* **2008**, *130*, 8706–8713.

(9) Weissleder, R.; Kelly, K.; Sun, E. Y.; Shtatland, T.; Josephson, L. Cell-Specific Targeting of Nanoparticles by Multivalent Attachment of Small Molecules. *Nat. Biotechnol.* **2005**, *23*, 1418–1423.

(10) Daniel, M.-C.; Astruc, D. Gold Nanoparticles: Assembly, Supramolecular Chemistry, Quantum-Size-Related Properties, and Applications toward Biology, Catalysis, and Nanotechnology. *Chem. Rev.* **2004**, *104*, 293–346.

(11) Grzelczak, M.; Pérez-Juste, J.; Mulvaney, P.; Liz-Marzán, L. M. Shape Control in Gold Nanoparticle Synthesis. *Chem. Soc. Rev.* **2008**, *37*, 1783–1791.

(12) Love, J. C.; Estroff, L. A.; Kriebel, J. K.; Nuzzo, R. G.; Whitesides, G. M. Self-Assembled Monolayers of Thiolates on Metals as a Form of Nanotechnology. *Chem. Rev.* **2005**, *105*, 1103–1169.

(13) Shan, J.; Tenhu, H. Recent Advances in Polymer Protected Gold Nanoparticles: Synthesis, Properties and Applications. *Chem. Commun.* **2007**, 4580–4598.

(14) Woehrle, G. H.; Brown, L. O.; Hutchinson, J. E. Thiol-Functionalized 1.5-nm Gold Nanoparticles through Ligand Exchange Reactions: Scope and Mechanism of Ligand Exchange. *J. Am. Chem. Soc.* **2005**, *127*, 2172–2183.

(15) Nativo, P.; Prior, I. A.; Brust, M. Uptake and Intracellular Fate of Surface-Modified Gold Nanoparticles. *ACS Nano* **2008**, *2*, 1639–1644.

(16) Chithrani, B. D.; Ghazani, A. A.; Chan, W. C. W. Determining the Size and Shape Dependence of Gold Nanoparticle Uptake into Mammalian Cells. *Nano Lett.* **2006**, *6*, 662–668.

(17) Kim, D.; Park, S.; Lee, J. H.; Jeong, Y. Y.; Jon, S. Antibiofouling Polymer-Coated Gold Nanoparticles as a Contrast Agent for in Vivo X-ray Computer Tomography Imaging. *J. Am. Chem. Soc.* **2007**, *129*, 7661–7665.

(18) Mirkin, C. A.; Letsinger, R. L.; Mucic, R. C.; Storhoff, J. J. A DNA-Based Method for Rationally Assembling Nanoparticles into Macroscopic Materials. *Nature* **1996**, *382*, 607–609.

(19) Hone, D. C.; Haines, A. H.; Russell, D. A. Rapid, Quantitative Colorimetric Detection of a Lectin Using Mannose-Stabilised Gold Nanoparticles. *Langmuir* **2003**, *19*, 7141–7144.

(20) Oishi, J.; Asami, Y.; Mori, T.; Kang, J.-H.; Niidome, T.; Katayama, Y. Colorimetric Enzymatic Activity Assay Based on Non-crosslinking Aggregation of Gold Nanoparticles Induced by Adsorption of Substrate Peptides. *Biomacromolecules* **2008**, *9*, 2301–2308.

(21) Zhou, Y.; Wang, S.; Zhang, K.; Jiang, X. Visual Detection of Copper(II) by Azide- and Alkyne-Functionalized Gold Nanoparticles Using Click Chemistry. *Angew. Chem., Int. Ed.* **2008**, *47*, 7454–7456.

(22) Guan, J.; Li, J.; Guo, Y.; Yang, W. Cooperative Dual-Stimuli-Triggered Aggregation of Poly-L-Histidine Functionalized Au Nanoparticles. *Langmuir* **2009**, *25*, 2679–2683.

(23) Raula, J.; Shan, J.; Nuopponen, M.; Niskanen, A.; Jiang, H.; Kauppinen, E. I.; Tenhu, H. Synthesis of Gold Nanoparticles Grafted with a Thermoresponsive Polymer by Surface-Induced Reversible-Addition-Fragmentation Chain-Transfer Polymerization. *Langmuir* **2003**, *19*, 3499–3504.

(24) Hussain, I.; Graham, S.; Wang, Z.; Tan, B.; Sherrington, D. C.; Rannard, S. P.; Cooper, A. I.; Brust, M. Size-Controlled Synthesis of Near-Monodisperse Gold Nanoparticles in the 1−4 nm Range Using Polymeric Stabilizers. *J. Am. Chem. Soc.* **2005**, *127*, 16398–16399.

(25) Lowe, A. B.; Sumerlin, B. S.; Donovan, M. S.; McCormick, C. L. Facile Preparation of Transition Metal Nanoparticles Stabilized by Well-Defined (Co)polymers Synthesized via Aqueous Reversible Addition-Fragmentation Chain Transfer Polymerization. *J. Am. Chem. Soc.* **2002**, *124*, 11562–11563.

(26) Wang, Z.; Tan, B.; Hussain, I.; Schaeffer, N.; Wyatt, M. F.; Brust, M.; Cooper, A. I. Design of Polymeric Stabilzers for Size-Controlled Synthesis of Monodisperse Gold Nanoparticles in Water. *Langmuir* **2007**, *23*, 885–895.

(27) Nuss, S.; Böttcher, H.; Wurm, H.; Hallensleben, M. L. Gold Nanoparticles with Covalently Attached Polymer Chains. *Angew. Chem., Int. Ed.* **2001**, *40*, 4016–4018.

(28) Bergen, J. M.; von Recum, H. A.; Goodman, T. T.; Massey, A. P.; Pun, S. H. Gold Nanoparticles as a Versatile Platform for Optimizing Physicochemical Parameters for Targeted Drug Delivery. *Macromol. Biosci.* **2006**, *6*, 506–516.

(29) Perrault, S. D.; Walkey, C.; Jennings, T.; Fischer, H. C.; Chan, W. C. W. Mediating Tumor Targetting Efficiency of Nanoparticles Through Design. *Nano Lett.* **2009**, *9*, 1909–1915.

(30) Gauthier, M. A.; Gibson, M. I.; Klok, H.-A. Synthesis of Functional Polymers by Post-Polymerization Modification. *Angew. Chem., Int. Ed.* **2009**, *48*, 48–58.

(31) *Sigma-Aldrich Fact Sheet Dulbecco's Modified Eagle's Medium (DMEM)* 2009.

(32) *Sigma-Aldrich Product Information M199* 2009.

(33) Haiss, W.; Thanh, N. T. K.; Aveyard, J.; Fernig, D. G. Determination of Size and Concentration of Gold Nanoparticles from UV-Vis Spectra. *Anal. Chem.* **2007**, *79*, 4215–4221.

(34) Gibson, M. I.; Fröhlich, E.; Klok, H.-A. Postpolymerization Modification of Poly(Pentafluorophenyl methacrylate): Synthesis of a Diverse Water-Soluble Polymer Library. *J. Polym. Sci., Part A: Polym. Chem.* **2009**, *47*, 4332–4345.

(35) Turkevich, J.; Stevenson, P. C.; Hillier, J. A Study of the Nucleation and Growth Processes in the Synthesis of Colloidal Gold. *Discuss. Faraday Soc.* **1951**, *11*, 55–75.

(36) Frens, G. Controlled Nucleation for the Regulation of the Particle Size in Monodisperse Gold Suspensions. *Nat. Phys. Sci.* **1973**, *241*, 20–22.

(37) Ghosh, S. K.; Pal, T. Interparticle Coupling Effect on the Surface Plasmon Resonance of Gold Nanoparticles: From Theory to Applications. *Chem. Rev.* **2007**, *107*, 4797–4862.

(38) Ratner, B.; Castner, D. In *Surface Analysis: The Principal Techniques*; Vickerman, J. C., Gilmore, I. S., Eds.; Wiley, Chichester, U.K., 2009.

(39) Joseph, Y.; Besnard, I.; Rosenberger, M.; Guse, B.; Nothofer, H.-G.; Wessels, J. M.; Wild, U.; Knop-Gericke, A.; Su, D.; Schlögl, R.; Yasuda, A.; Vossmeyer, T. Self-Assembled Gold Nanoparticle/Alkanedithiol Films: Preparation, Electron Microscopy, XPS-Analysis, Charge Transport, and Vapor-Sensing Properties. *J. Phys. Chem. B* **2003**, *107*, 7406–7413.

(40) Kim, T.; Lee, K.; Gong, M.-S.; Joo, S.-W. Control of Gold Nanoparticle Aggregates by Manipulation of Interparticle Interaction. *Langmuir* **2005**, *21*, 9524–9528.

(41) Ohshima, H. A Simple Expression for Henry's Function for the Retardation Effect in Electrophoresis of Spherical Colloidal Particles. *J. Colloid Interface Sci.* **1994**, *168*, 269–271.

(42) Boyer, C.; Whittaker, M. R.; Chuah, K.; Liu, J.; Davis, T. P. Modulation of the Surface Charge on Polymer-Stabilized Gold Nanoparticles by the Application of an External Stimulus. *Langmuir* **2010**, *26*, 2721–2730.

(43) Hussain, I.; Brust, M.; Barauskas, J.; Cooper, A. I. Controlled Step Growth of Molecularly Linked Gold Nanoparticles: From Metallic Monomers to Dimers to Polymeric Nanoparticle Chains. *Langmuir* **2009**, *25*, 1934–1939.

(44) Tugulu, S.; Arnold, A.; Sielaff, I.; Johnsson, K.; Klok, H.-A. Protein-Functionalized Polymer Brushes. *Biomacromolecules* **2005**, *6*, 1602–1607.